

# Partial Volume Simulation in Software Breast Phantoms

Feiyu Chen, David Pokrajac, Xiquan Shi, Fengshan Liu,  
Andrew D.A. Maidment<sup>a</sup>, Predrag R. Bakic<sup>a</sup>

Delaware State University, 1200 N DuPont Hwy, Dover DE 19904;  
<sup>a</sup>University of Pennsylvania, 3400 Spruce Street, Philadelphia, PA 19104

FChen09@students.desu.edu, {DPokrajac, XShi, FLiu}@desu.edu,  
{Andrew.Maidment, Predrag.Bakic}@uphs.upenn.edu

## ABSTRACT

A modification to our previous simulation of breast anatomy is proposed, in order to improve the quality of simulated projections generated using software breast phantoms. Anthropomorphic software breast phantoms have been used for quantitative validation of breast imaging systems. Previously, we developed a novel algorithm for breast anatomy simulation, which did not account for the partial volume (PV) of various tissues in a voxel; instead, each phantom voxel was assumed to contain single tissue type. As a result, phantom projection images displayed notable artifacts near the borders between regions of different materials, particularly at the skin-air boundary. These artifacts diminished the realism of phantom images. One solution is to simulate smaller voxels. Reducing voxel size, however, extends the phantom generation time and increases memory requirements. We achieved an improvement in image quality without reducing voxel size by the simulation of PV in voxels containing more than one simulated tissue type. The linear x-ray attenuation coefficient of each voxel is calculated by combining attenuation coefficients proportional to the voxel subvolumes occupied by the various tissues. A local planar approximation of the boundary surface is employed, and the skin volume in each voxel is computed by decomposition into simple geometric shapes. An efficient encoding scheme is proposed for the type and proportion of simulated tissues in each voxel. We illustrate the proposed methodology on phantom slices and simulated mammographic projections. Our results show that the PV simulation has improved image quality by reducing quantization artifacts.

**Keywords:** Digital mammography, anthropomorphic breast phantom, partial volume simulation, computational geometry.

## 1. INTRODUCTION

We propose to modify our method for generating software breast phantoms by simulating the partial volume (PV) of various materials contained in a voxel. Our aim is to improve the quality of synthetic x-ray projections of the phantom. The current method for simulating the breast anatomy<sup>1</sup> assumes that each voxel contains a single tissue type, which causes notable artifacts due to abrupt attenuation transitions at the borders between regions of different simulated materials. The realism of the resulting phantom images is thus reduced. The realism can be improved by using a smaller voxel size. Reducing the voxel size, however, extends the phantom generation time and increases memory requirements. It should be possible to improve image quality without reducing voxel size by explicitly accounting for simulating voxels containing more than one simulated tissue type. We have implemented this PV strategy on the skin/air boundary, and have qualitatively validated the improvement in image quality. In this paper we present an overview of the method and propose efficient representation for the PV proportion values. The results are illustrated using slices and simulated projections of phantoms with simulated PV.

In this paper a method is proposed to simulate PV averaging in the software breast phantoms developed at the University of Pennsylvania. Most current software breast phantoms<sup>2-5</sup> do not account for PV; they assume each voxel belongs to one predefined class of simulated materials (e.g., skin, adipose tissue, fibroglandular [dense] tissue, microcalcifications, and air. Methods for voxel assignment depend on the type of the phantom. For phantoms generated based upon the rules for simulating anatomical structures, those rules result in a discretized material type to be assigned to phantom voxels.<sup>1,2,5</sup> For phantoms generated based upon the use of individual clinical images, the

voxel assignment is made by the segmentation of clinical data into one of the predefined classes of simulated materials.<sup>3, 4, 6</sup>

The PV is indirectly simulated in one of the phantom generation methods developed at the University of Massachusetts.<sup>6</sup> There, each voxel of reconstructed breast CT images of mastectomy specimens has been scaled into a value from 0.01 to 0.99. The voxel values are interpreted as percentage of adipose tissue contained in the voxel. The scaling method resulted in phantom images more similar to the original CT data, as compared to the method based upon the segmentation into discrete tissue types. The scaling helped to preserve some of the fine tissue structure which would be lost when using the segmentation; however, it resulted in more noisy images.

In the proposed method, the partial volume of each voxel occupied by different materials is computed first. The linear attenuation coefficient is assigned as the linear combination of attenuations weighted by the partial volume occupied by each material in the voxel. Once the partial volume of each voxel which contain different materials is computed, the results can be used not only to measure the attenuation, but also to keep track of the proportion of different materials and their composition in the voxel. In addition, the paper discusses an encoding technique to accomplish efficient storage of the material composition.

## 2. METHODOLOGY

### 2.1 Partial Volume Simulation

PV support is necessary when a voxel in a 3-D model contains more than one attenuating material. For example, in our software breast phantom<sup>1</sup>, a voxel may contain a mixture of adipose and dense (fibroglandular) tissues (see Fig. 1). In this paper the equivalent linear attenuation coefficient  $\mu_V$  of the voxel is computed as a combination of the linear attenuation coefficients of different tissues, proportional to partial volumes of the individual tissue types:

$$\mu_V = \frac{1}{|V|} \sum_i \mu_i |V_i| \quad (1)$$

where  $|V_i|$  is measure of volume occupied by material  $i$  associated to the linear x-ray attenuation  $\mu_i$ , and  $|V|$  is the measure of the voxel volume. The linear attenuation coefficient of the voxel is calculated as:

$$\mu_V = \sum_i \mu_i p_i, \quad (2)$$

where  $p_i$  is the percentage of the material  $i$  in the voxel, defined as:

$$p_i = \frac{|V_i|}{|V|} \times 100\%. \quad (3)$$

In general, a voxel may contain multiple materials. However, when simulating images with controlled thickness of the septa, the maximal number of materials per voxel may be reduced. In our specific case, when the voxel size is smaller than the simulated thicknesses of both the skin and Cooper's ligaments, a voxel contains up to three materials. Hence, the following cases of PV can be distinguished, (Fig 2): (1) skin and air; (2) Cooper's ligament and dense tissue; (3) Cooper's ligament and fat tissue; (4) dense tissue and skin; (5) fat and skin; (6) skin, dense tissue and Cooper's ligament; (7) skin, fat and Cooper's ligament.

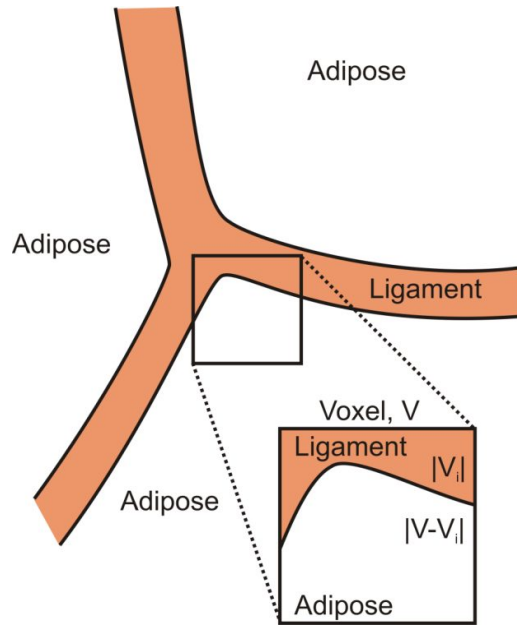


Figure 1: Concept of partial volume computation:  $V$  denotes the voxel and  $V_i$  is the sub volume occupied by dense tissue.

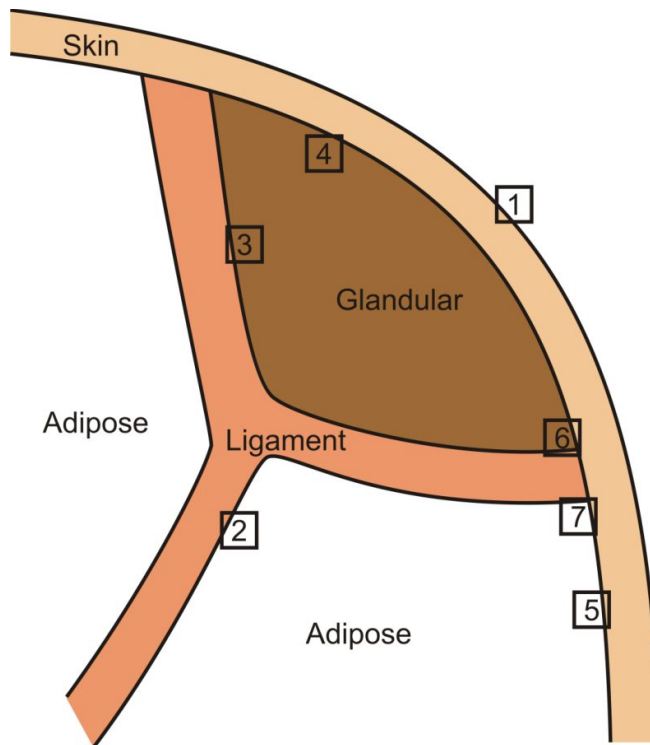


Figure 2: 2D illustration of possible PV cases.

### 2.1.1 Linear Approximation

In this paper, we demonstrate the effect of PV on the skin/air boundary. This boundary contributes to high contrast features in the image, due to the large difference in linear attenuation coefficients between the air and breast tissue (i.e., the skin). We assume that the outer surface of the skin is defined by function  $f_s(\mathbf{x}) = 1$ , such that each point in the air satisfies  $f_s(\mathbf{x}) > 1$ . The function  $f_s(\mathbf{x})$  is given by the following formula:

$$f_s(\mathbf{x}) = \begin{cases} 1, & x < 0 \\ \frac{x^2}{a^2} + \frac{y^2}{b^2} + \frac{z^2}{c'^2}, & x > 0, z \geq 0, \\ \frac{x^2}{a^2} + \frac{y^2}{b^2} + \frac{z^2}{c''^2}, & x > 0, z < 0. \end{cases} \quad (4)$$

Points  $\mathbf{x}$  from a voxel  $V$  below the skin satisfy  $V_i = \{\mathbf{x}: \mathbf{x} \in V, f_s(\mathbf{x}) < 1\}$ . When  $f_s(\mathbf{x})$  is known in a closed form, the volume  $|V_i|$  can be calculated; however, the exact calculation of this quantity is computationally inefficient. Instead, the function  $f_s(\mathbf{x})$  is approximated by a tangent plane  $\pi$  which reduces the problem to computation of the voxel volume below a tangent plane. The tangent plane  $\pi$  on the surface  $f_s(\mathbf{x}) = 1$  is placed at a point  $\mathbf{x}_0$  inside the voxel  $V$ . The point  $\mathbf{x}_0$  satisfies  $f_s(\mathbf{x}) = 1$  and is on the line segment between the points  $\mathbf{x}_m$  and  $\mathbf{x}_M$ . The points  $\mathbf{x}_m$  and  $\mathbf{x}_M$  are calculated such that  $\mathbf{x}_m = \arg \min_V f_s(\mathbf{x})$ , and  $\mathbf{x}_M = \arg \max_V f_s(\mathbf{x})$ . Points  $\mathbf{x}$  on the tangent plane  $\pi$  satisfy the condition  $(\mathbf{x}_m - \mathbf{x}_M) \cdot \mathbf{N} = 0$ , where “ $\cdot$ ” denotes the scalar product and  $\mathbf{N} = \nabla f_s(\mathbf{x}_0)$  is the gradient vector at the point  $\mathbf{x}_0$  (See Fig. 3).

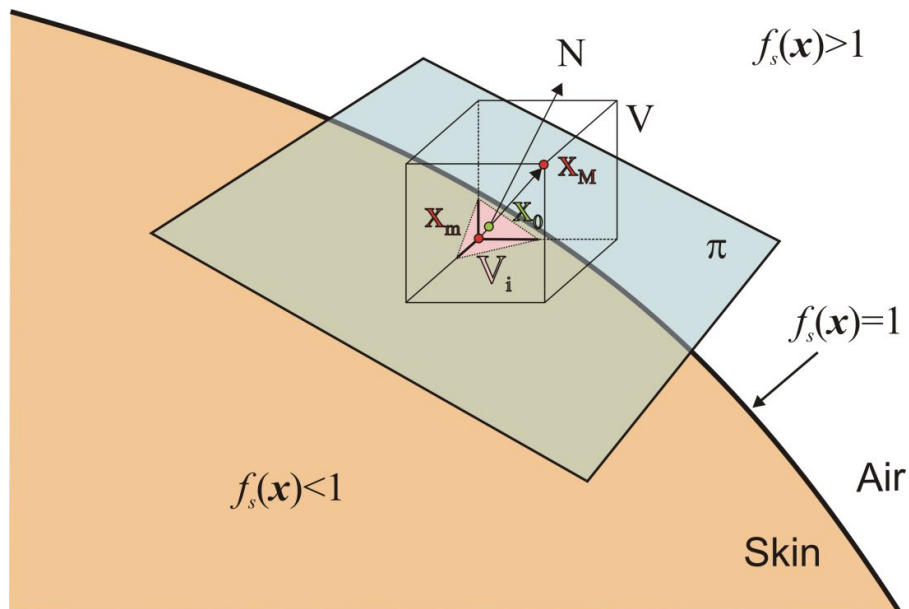


Figure 3: Local approximation of skin boundary (defined by a tangent plane  $f_s(\mathbf{x})=1$ ).

### 2.1.2 Calculation of the Partial Volume

In this section, a fast and accurate method is proposed to determine the fraction of the volume  $V$  which is located below the plane  $\pi$ . The number  $s$  of vertices located above the plane is determined first. A vertex  $\mathbf{x}_i$  which is above  $\pi$  satisfies the inequality:

$$(\mathbf{x}_i - \mathbf{x}_0) \cdot \mathbf{N} > 0 \quad (5)$$

Intersections of the plane  $\pi$  and the voxel surface are computed as follows. Assume the point  $\mathbf{x}$  is the intersection of  $\pi$  and the voxel surface. Then,  $\mathbf{x}$  can be expressed as the linear combination of  $\mathbf{x}_i$  and  $\mathbf{x}_j$ , i.e.,  $\mathbf{x} = \mathbf{x}_i + t(\mathbf{x}_i - \mathbf{x}_j)$ ,  $t \in [0,1]$ , where  $[\mathbf{x}_i, \mathbf{x}_j]$  is an edge of the cube. On the other hand, the point  $\mathbf{x}$  satisfies the plane equation:  $(\mathbf{x} - \mathbf{x}_0) \cdot \mathbf{N} = 0$ . The parameter  $t$  is obtained from:

$$t = \frac{(\mathbf{x}_i - \mathbf{x}_0) \cdot \mathbf{N}}{(\mathbf{x}_i - \mathbf{x}_j) \cdot \mathbf{N}}. \quad (6)$$

Thus, all the intersection points can be obtained by computing only inner vector products. Finally, some edges of the cube can be extended to construct fundamental shapes, such as prisms and pyramids, with vertices comprised of the intersection points and voxel vertices. The partial volume is subsequently computed by evaluating volumes of the fundamental shapes, see Fig. 4.

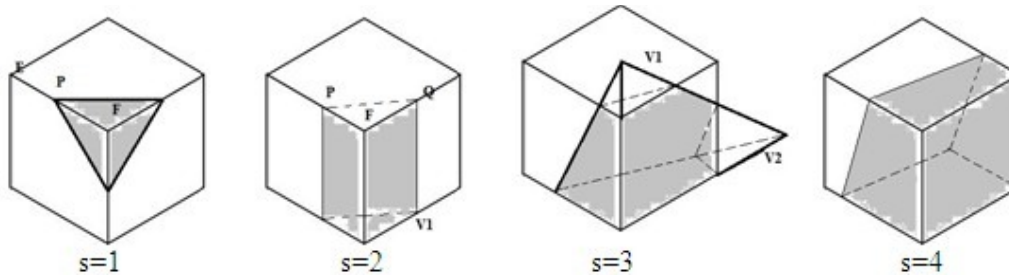


Figure 4: Illustration of some cases (out of the 8 possible) for plane/voxel combinations when calculating PV.  $s$  denotes number of vertices above the plane.

## 2.2 Method for Image Simulation

To demonstrate the benefits of the partial volume simulation, x-ray projections were simulated through uncompressed phantoms with and without simulated partial volume. The x-ray image acquisition was simulated assuming a monoenergetic x-ray beam (corresponding to 20 kVp), and a parallel x-ray propagation. An ideal x-ray detector model was assumed, with the distance between detector elements equal to 70 microns. No scatter or quantum noise was simulated. Images were simulated at different voxel sizes with and without partial volume. Images were compared in terms of qualitative appearance and artifacts.

## 2.3 Material Encoding Scheme

For efficient storage of the PV information, we propose a representation of material type and PV composition using a two-byte binary word. The voxel label of the major type of material associated with the voxel is stored, as well as percentages of the voxel volumes for two minor tissue types. Since a voxel size smaller than the thickness of the skin or Cooper's ligaments is assumed, it is sufficient to consider combinations of up to three materials in a voxel. Thus, the percentage of the major material type is obtained by subtracting percentages of the minor materials from 100%.

An encoding scheme is proposed where the two least significant bits are used to indicate the major material label. The percentages of minor materials are stored as two 7-bit records containing discretized percentages  $p_1$  and  $p_2$  (see Table 1). The label also determines two materials to which  $p_1, p_2$  correspond. The percentage  $p_0$  of the major material can be obtained as

$$p_0 = 100 - p_1 - p_2. \quad (7)$$

The label values corresponding to the possible major simulated materials are: 0 (skin or air); 1 (Cooper's ligaments), 2 (fat/skin boundary) and 3 (dense/skin boundary). For example, consider the case, when the label=0 (skin/air boundary). Here,  $p_1$  corresponds to fat tissue (with a constant value 0 in air/skin voxels!), while  $p_2$  corresponds to the ratio  $|V - V_i|/|V|$ . The percentage  $p_0$  of skin, as the major material, can be obtained from Eq. (7). The proposed representation also covers the cases when a voxel is comprised of a single material (e.g., a voxel belonging entirely to skin would have label 0 and  $p_1=p_2=0$ ).

Table 1: Material combinations for PV simulation and their encoding with a 2-byte descriptor.

Case	$p_1$ (7 bits)	$p_2$ (7 bits)	Label (2 bits)
1. Skin and air	0	$p_{Air}$	0
2. Cooper's ligament; fat	$p_{Fat}$	0	1
3. Cooper's ligament; dense	0	$p_{Dense}$	1
4. Skin; dense tissue	0	$p_{Skin}$	3
5. Skin; fat tissue	0	$p_{Skin}$	2
6. Skin, Cooper's ligament and dense tissue	$p_{Cooper}$	$p_{Skin}$	3
7. Skin, Cooper's ligament and fat tissue	$p_{Cooper}$	$p_{Skin}$	2

### 3. RESULTS

Fig. 5 illustrates the effect of partial volume on skin/air boundary of a 450ml software breast phantom, simulated with 400 $\mu$ m voxels. A detail of the phantom is presented magnified to show more detailed view on skin and air. Displayed is the percentage of skin tissue on the skin/air boundary. Fig. 5 demonstrates that the percentage of skin in PV voxels decreases with the distance from the inner part of skin, such that voxels closer to the air contain smaller percentages of skin.

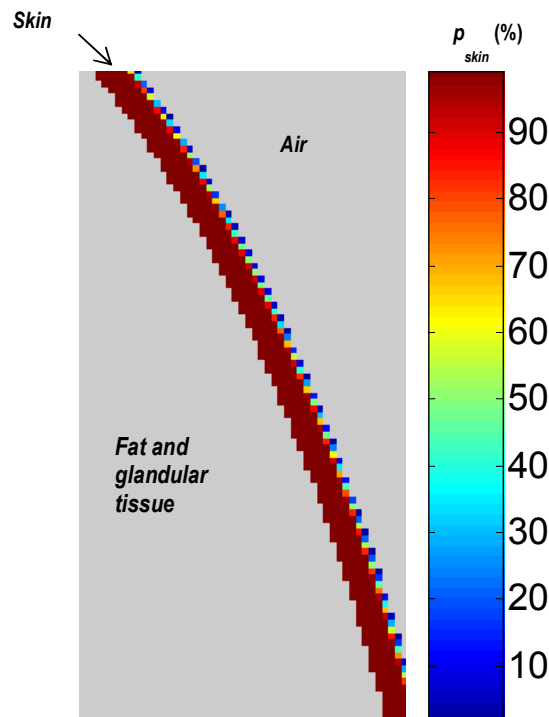


Figure 5: Detail of a 400 $\mu$ m phantom with percentage of skin tissue in the voxels on the skin/air border.

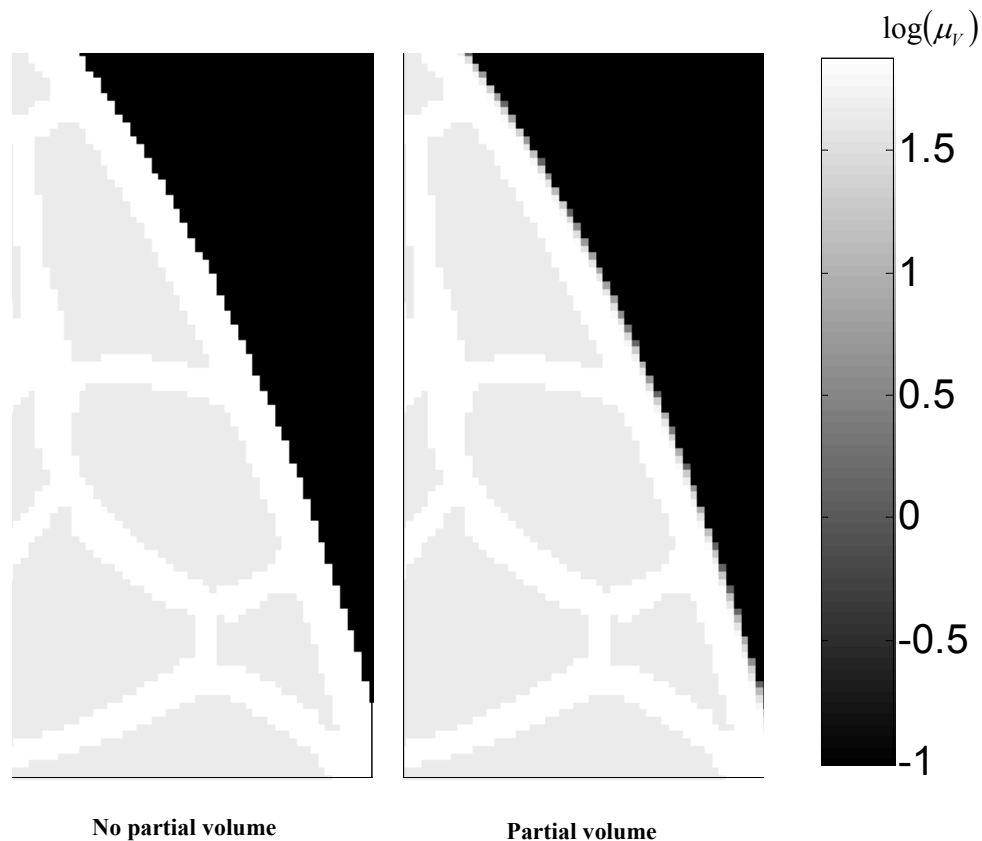


Figure 6: Details of breast phantoms with 400 $\mu\text{m}$  voxels, without (left) and with (right) PV simulation.

Fig. 6 illustrates the effect of simulating in PV in voxels near skin/air boundary on the phantom x-ray attenuations. Shown are details of phantom sections with and without PV simulation. The intensity scale corresponds to the logarithms of voxel linear attenuation coefficients. In Fig. 6, the voxel attenuation coefficients are shown to gradually change on the skin/air boundary (instead of having only two values of simulated attenuation coefficients as in a phantom with no PV simulation). This way, the transitions of voxel attenuation coefficients near the edge of the phantom are smoother. Also, as expected, the boundary voxels closer to the inner part of skin have higher attenuation coefficients.

Fig. 7 illustrates detail of a breast phantom with 400 $\mu\text{m}$  voxels, (a) without and (b) with PV support, as compared with corresponding phantoms (c) with 200 $\mu\text{m}$  voxels without PV support and (d) with 100 $\mu\text{m}$  voxels without PV support. The figure shows that the PV simulation can reduce the notable artifacts caused by an abrupt change of attenuation between skin and air regions. As indicated in Fig. 7(a), such linear artifacts are visible on phantom with 400 $\mu\text{m}$  voxels with no partial volume implemented. Albeit to smaller extent, the artifacts are also present at phantom with 200 $\mu\text{m}$  voxels, Fig. 7(c) and gradually disappear with the higher resolution, Fig. 7(d). In contrast, the 400 $\mu\text{m}$  phantom with PV implemented, Fig. 7(b), does not have linear artifacts. This contributes to its higher realism. Hence, the application of PV can lead to improved quality of synthetic images of the phantom, with reduced stepwise discretization artifacts.

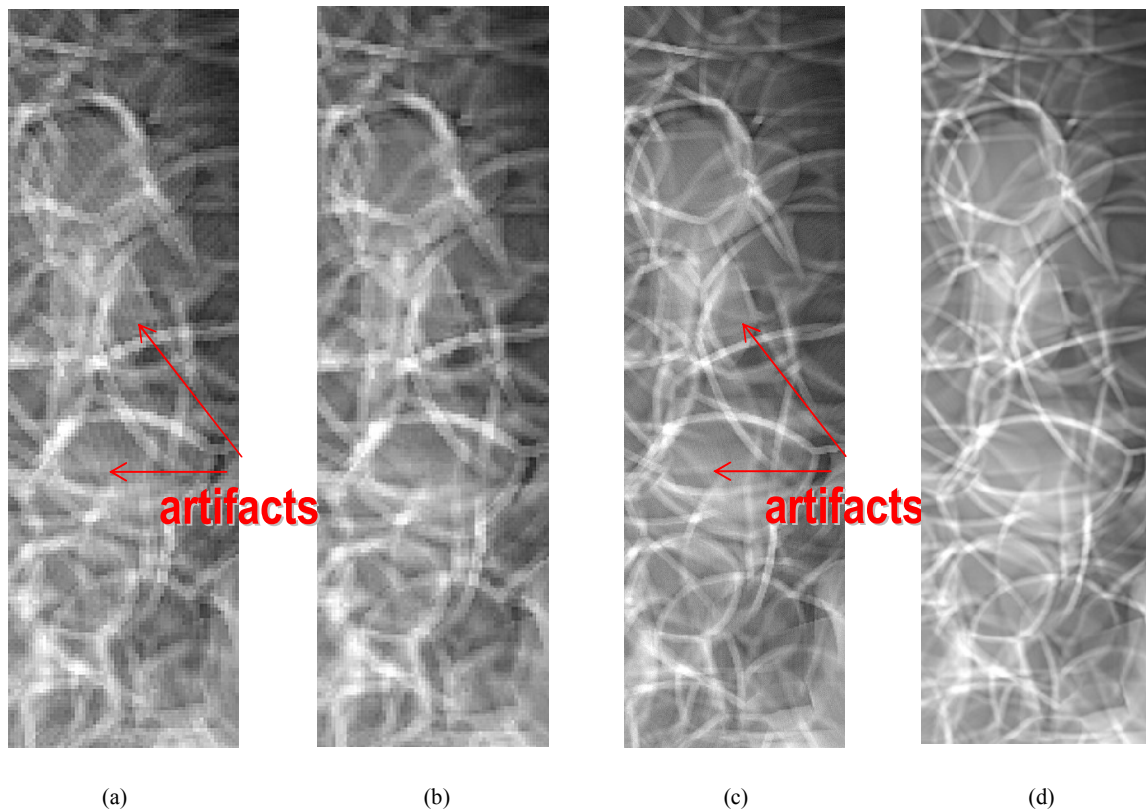


Figure 7: Details of simulated parallel X-ray projections of the phantoms: (a) 400µm voxels, no partial volume; (b) 400µm voxels, partial volume; (c) 200µm voxels, no partial volume; (d) 100µm voxels, no partial volume.

#### 4. DISCUSSION

The purpose of this project was to demonstrate the ability to simulate PV. The proposed method was demonstrated to improve the quality of simulated images by better representation of voxels containing two materials. We have identified several limitations of the presented work. Only one possible case (skin/air boundary) was considered, which has the largest difference in linear attenuation coefficients between the materials (air and tissue) and hence potentially the largest impact on the image quality. The proposed technique can be applied into other cases of two materials, such as case 4 and case 5 (skin/adipose tissue and skin/glandular tissue) in Fig. 2. To apply the methodology in cases 2 and 3 (Cooper's ligament/glandular tissue and Cooper's ligament/adipose tissue) a proper method to determine the planar approximation of the Cooper's ligament boundary is needed. Further, a method can be developed that allows simulation of voxels with three materials (cases 6, 7). Such a method would involve linear approximation of multiple material boundaries and computation of PV of voxels determined by the two intersecting planes.

The proposed method utilizes planar approximation of the surface at the materials' boundary. While this approximation is computationally efficient, more accurate results could be obtained by using the quadratic functions to represent the boundaries.

Note that the paper considers a parallel beam projection of uncompressed phantom with no quantum noise simulated. Such a simplified acquisition setup allows validating the benefits of the PV simulation, separately from the effect of other factors influencing the image quality. Our work in progress includes developing techniques that perform realistic simulation of mammography image acquisition of the PV phantoms. This way, the influence of the proposed technique on quality of simulated images can be better evaluated.

The present paper provides only qualitative measures of the image improvements achievable using the proposed PV simulation. Our work in progress includes development and application of objective measures to quantify the image enhancement due to the proposed technique. Specifically, these measures would help elucidate the trade-off between PV simulation vs. increasing voxel resolution of the phantom. Also, we are working on validating the computed voxel linear attenuation coefficients by subdividing a phantom. In this method, a series of non-PV phantoms equivalent to the considered phantom at progressively higher resolutions can be simulated. The equivalent attenuation coefficients for a voxel from the original phantom can be estimated by averaging attenuations from corresponding voxels of a high resolution phantom.

We anticipate that more theoretical work is needed to determine the influence of the voxel size of the simulated 3D models on the quality of the simulated images. For example, the influence of the PV simulation on reducing quantization artifacts can be explored using properties of 3D Fourier spectrum of the simulated structure.

The conversion from the current approach based upon the discrete representation of materials simulated in each voxel to a simulation of material mixture is a complex change. The success of our partial volume simulation will impact the breast compression and image acquisition simulation steps. Developing a breast imaging simulation chain completely based upon the multiple material simulations is one of our research aims for the near future.

## 5. CONCLUSIONS

We have proposed a method to compute PV of voxels in simulated breast phantoms that correspond to different materials. The methodology was demonstrated by simulation of voxels on the skin/air boundary. The results indicate that the proposed method can improve the quality of simulated images, while retaining the same voxel size, or, conversely, it could allow for simulations using larger phantom voxels for a required image quality. Work in progress includes implementation of PV simulation when voxels contain three materials and investigating the influence of linear approximation on the accuracy of the method.

## 6. ACKNOWLEDGMENT

This work was supported in part by the US Department of Defense Breast Cancer Research Program (HBCU Partnership Training Award #BC083639), the US National Institutes of Health (R01 grant #CA154444), the US National Science Foundation (CREOSA grant #HRD-0630388), and the US Department of Defense/Department of Army (45395-MA-ISP, #54412-CI-ISP). The authors would like to thank Ms. Susan Ng from Real-Time Tomography (Villanova, PA) for processing the simulated projection images.

## REFERENCES

1. Pokrajac DD, Maidment ADA, Bakic PR. A Method for Fast Generation of High Resolution Software Breast Phantoms. *Medical Physics*. 2011;38:3431.
2. Bliznakova K, Suryanarayanan S, Karellas A, Pailikarakis N. Evaluation of an improved algorithm for producing realistic 3D breast software phantoms: Application for mammography. *Medical Physics*. 2010;37(11):5604-5617.
3. Hoeschen C, Fill U, Zankl M, Panzer W, Regulla D, Dohring W. A high resolution voxel phantom of the breast for dose calculations in mammography. *Radiation Protection Dosimetry* 2005;114(1-3):406-409.
4. Li CM, Segars WP, Tourassi GD, Boone JM, Dobbins III JT. Methodology for generating a 3D computerized breast phantom from empirical data. *Medical Physics*. 2009;36(7):3122-3131.
5. Chen B, Shorey J, Saunders RSJ, et al. An anthropomorphic breast model for breast imaging simulation and optimization. *Academic Radiology*. 2011;18(5):536-546.
6. O'Connor JM, Das M, Didier C, Mah'D M, Glick SJ. Comparison of two methods to develop breast models for simulation of breast tomosynthesis and CT. In: Krupinski EA, ed. *Digital Mammography (IWDM)*. Vol 5116. Berlin-Heidelberg: Springer-Verlag; 2008:417-425.